UNIFORMITY INDEX AS A UNIVERSAL AIR-COOLED CONDENSER FAN PERFORMANCE METRIC

Fredrik S. MARINCOWITZ[1], Michael T. F. OWEN[1],
Jacques MUIYSER[2], Peter HOLKERS[2]

[1] *Stellenbosch University, Mechanical Department, Private Bag X1, Matieland, Stellenbosch 7602, South Africa*

[2] *Howden Netherlands, Haaksbergerstraat 67, Hengelo 7554 PA, Netherlands*

SUMMARY

This paper presents air-cooled condenser fan inlet airflow uniformity index as a metric that can estimate the severity of the reduction in fan volumetric performance and the increase in dynamic blade loading under windy conditions. Based on both numerical simulation and on-site experimental data, uniformity index was shown to have a proportional relationship with fan volumetric effectiveness and dynamic blade loading.

INTRODUCTION

Background

Mechanical forced-draft direct air-cooled steam condensers (ACCs) are widely employed as a condenser technology in thermal energy system. ACCs use large axial fans to force ambient air through A-frame heat exchangers (Figure 1) and reject the required heat load and maintain the turbine backpressure at or near the design point. The thermal performance of an ACC is directly influenced by ambient wind, causing a reduction in fan volumetric performance with increasing wind speed [1]. Furthermore, ACC thermal performance is indirectly influenced by ambient wind due to increased dynamic fan blade loading of the upwind edge fans, which can result in physical damage to the fan blades [2] and subsequent downtime for repairs.

Wind effects on ACC fans are caused by an increase in the horizontal velocity component (cross-flow) of the air moving beneath the fan platform under windy conditions. High cross-flow past the fan inlets causes distortions in the inlet flow distribution [3]. The non-uniform inlet flow distribution negatively affects the fans' ability to deliver their rated air volume flow rate [3] and

results in a variation in aerodynamic loading on the fan blades as they rotate through the non-uniform flow field [4]. There are two types of cross-flow related inlet flow distortions identified in the literature: flow separation at the fan inlet [3,5] and off-axis inflows [6,7] (shown in Figure 1). The flow separation at the fan inlet is considered the dominant cause of the wind-related degradation in fan volumetric performance [3] and increases to dynamic fan blade loading [8].

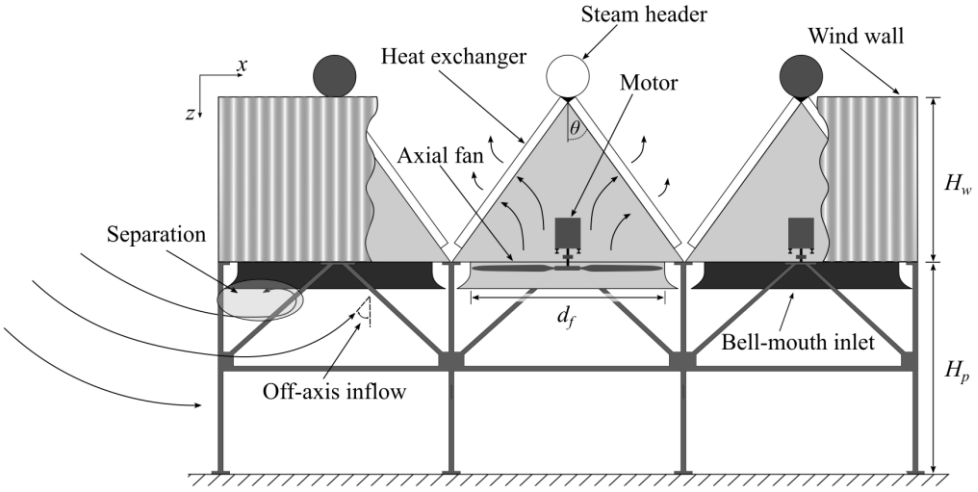

Figure 1: ACC schematic showing primary components and wind effects

On-site measurement of ACC fan volumetric performance is done using propeller anemometers placed at various radial and tangential locations on the fan's inlet safety grid [2,9]. These anemometers are used to measure the axial velocity at these fixed locations within the fan inlet and are subsequently used to calculate the volume flow rate or average axial velocity through the fan. The CTI-PTG-143 standard [10] recommends 40 anemometer measurements (four quadrants with ten measurements at equal radial spacing per quadrant) for fans with diameters exceeding 20 ft., as is common in ACCs (typically around 36 ft.). This makes continuous measurement of on-site airflow difficult as the process requires a large amount of measuring equipment. On the other hand, dynamic fan blade loading can be accurately evaluated using bending strain measurements, typically using strain gauges attached to the root of a fan blade in a full-bridge configuration [9]. This requires access to the fan blades and for the fan to be stopped, which is not always possible at an operational plant.

Wind effects on ACC performance are often investigated numerically using computational fluid dynamics (CFD) [11,12] due to the limitations of on-site measurements (uncontrollable environmental variables, specialist measurement equipment, site-specific results, and the difficulties of accurately measuring on-site wind speed). Most numerical studies tend to focus on fan volumetric performance due to the challenges related to the prediction of dynamic blade loading. Dynamic blade loading can, however, be approximated numerically. This has been done by either utilising a blade element theory-based fan model that makes it possible to calculate a flap-wise bending moment distribution [7,13] or by analysing the variation in static pressure within the fan rotational plane [14]. Of the two methods, only the flap-wise bending moment distribution method has been directly evaluated against experimental blade loading trends [15].

Motivation and aim

Literature relating to ACC fans and wind effects includes numerical and experimental studies that tend to focus on either volumetric performance or dynamic blade loading due to the difficulties related to determining the former in experimental work and the latter in numerical work. That these performance metrics are related is implicit since they are both affected by the same phenomena (distorted inflow).

Laboratory research [8] has indicated that the uniformity of the axial velocity inflow of a fan could be used to indicate the severity of dynamic blade loading. Furthermore, the uniformity of the axial velocity should have a proportional relationship with the average axial velocity of the fan, as the axial velocity inflow distribution infers the state of the fan's volumetric performance. For a uniform distribution, the fan is likely to be operating close to design conditions. As a result, the fan's inflow uniformity was identified as a metric of interest.

This study used a numerical CFD-based approach to investigate the relationship between ACC fan inflow uniformity, quantified by means of a uniformity index (Eq. (3)) and both fan volumetric performance and dynamic blade loading under windy conditions. The numerical correlations were also validated against on-site experimental test data obtained from a third party.

NUMERICAL MODELING

Numerical ACC model

A brief overview of the numerical CFD-based model is given in this section. The ACC model consisted of 3 × 6 simplified fan cells (depicted in Figure 2 (b)), with each cell consisting of an axial flow fan, an A-frame heat exchanger and a steam supply duct. Figure 3 shows the component configuration and numerical mesh that was used for the fan cells.

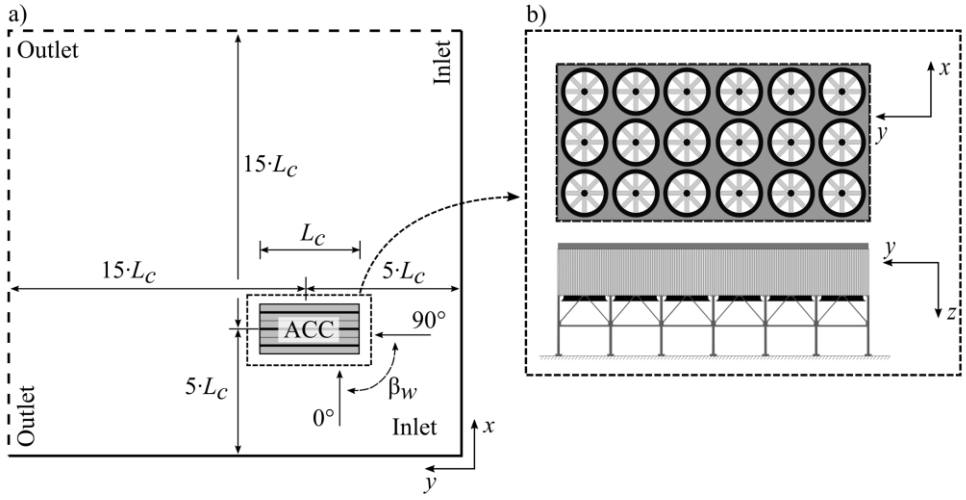

Figure 2: (a) Top view of the computational domain and (b) the 3 × 6 fan array layout

The 3 × 6 cell ACC was placed in the flow domain shown in Figure 3 (a). The figure indicates the inlet and outlet boundaries, as well as the wind direction definition (β_w). The wind speed (v_w) and direction range investigated with the numerical model were $1 \leq v_w \leq 11$ m/s and $-90^\circ \leq \beta_w \leq 90^\circ$. The domain dimensions are based on Franke *et al.*'s [16] recommendations for computational modelling for wind engineering purposes. The ACC's longest dimension was used as a conservative characteristic length (L_c) with a domain height (z-direction) of 6 L_c. Richards and Hoxey's [17] atmospheric wind boundary condition was used in the numerical model. They define the profiles for the z-velocity, turbulent kinetic energy and dissipation rate needed to simulate a horizontally homogeneous turbulent atmospheric boundary layer when using a k-ε turbulence model. The k-ε realizable turbulence model was used in this study which is consistent with other numerical studies in this research field [18,19].

The heat exchangers were modelled using porous media zones with appropriate momentum sink and energy source terms to replicate the finned tube heat exchangers' flow resistance and heat transfer rate. The momentum sink terms for the x, y and z momentum equations were defined by the Darcy Forcheimer equation with the viscous and inertial loss coefficients derived from empirical

pressure loss coefficients correlations obtained from [20]. The energy source term was calculated using the effectiveness-number of transfer units method of heat exchanger analysis [21].

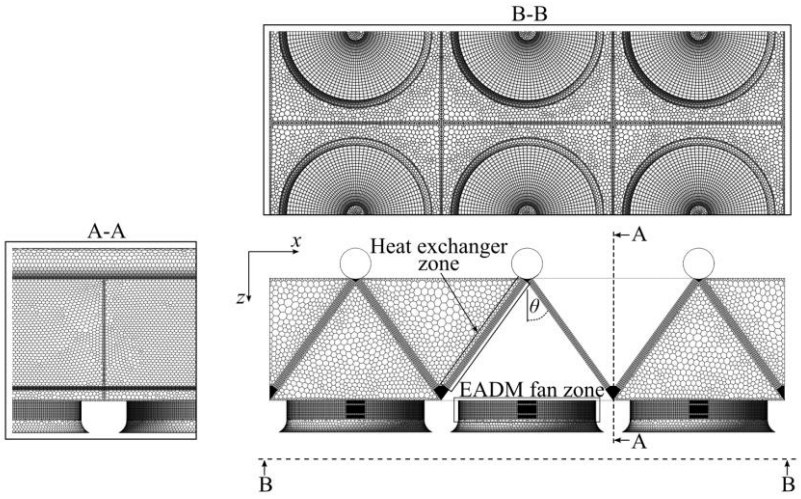

Figure 3: Numerical fan and heat exchanger mesh

The axial flow fans of the ACC were all modelled using the Extended Actuator Disk Fan Model (EADM) (described in detail in the following section), as was used by Venter *et al.* [19] and Engelbrecht *et al.* [18]. The axial flow fans modelled were based on a commercially available industrial axial fan. Table 1 lists some of the specifications for this fan. For more specific details on the numerical model such as solver settings and grid sensitivity analysis refer to [22].

Table 1: Axial fan specifications

Parameter name		Value
Fan diameter	d_f	10.363 m
Hub diameter	d_h	1.4 m
Number of blades	n_b	9
Rotational speed	N	93.2 rpm
Design flow rate[a]	$\dot{V}$	576.54 m³/s
Design pressure rise[a]	p	119.8 Pa

[a]At a reference air density of ρ_a = 1.22 kg/m³

Axial fan model

The EADM (see [23] for a full description) is an adaptation of the blade element theory-based actuator disk model [4]. The EADM is implemented into a structured grid region, with single element thickness and n_r = 20 radial and n_θ = 120 tangential divisions, representing the fan's rotor (see Figure 2 plane B-B). Each grid element of the rotor region is approximated as a two-dimensional aerofoil (blade element) with lift (δL) and drag (δD) forces dependant on the relative velocity (w_m) and the lift (C_L) and drag (C_D) coefficients of the blade element's aerofoil profile. The relative velocity is calculated from the incoming velocity vector ($\mathbf{v}_m$) and the tangential velocity ($\Omega\, r$). The lift and drag forces are introduced into the solver's momentum equations as axial (Eq. (1)) and tangential (Eq. (2)) source terms. Figure 4 shows the velocity vectors and force directions for a single blade element.

$$S_z = \frac{-\delta f_z}{\delta V} = -\frac{1}{2}\rho\, w_m^2\, \frac{\sigma}{t}\,(C_L \cos\beta_m - C_D \sin\beta_m) \tag{1}$$

$$S_\theta = \frac{\delta f_\theta}{\delta V} = \frac{1}{2}\rho\, w_m^2\, \frac{\sigma}{t}(C_L \sin\beta_w + C_D \cos\beta_w) \tag{2}$$

where β_m is the relative velocity angle shown in Figure 4, t is rotor-zone thickness, ρ is the fluid density and σ is the blade solidity.

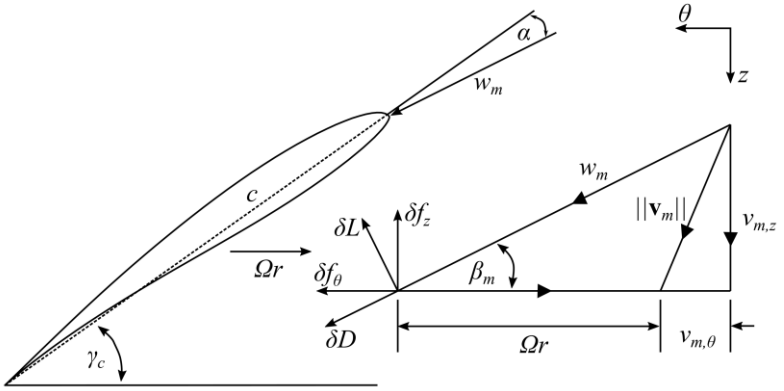

Figure 4: EADM vector diagram

Numerical evaluation metrics

The variation in the axial velocity within the fan rotor region is quantified using a uniformity index (γ_i) as given by Eq. (3) [24]. A uniformity index of unity represents perfectly uniform flow.

$$\gamma_i = 1 - \frac{\sum_{k=1}^{n_r}\sum_{j=1}^{n_\theta}|v_{z,kj} - \bar{v}_{Az}|A_{z,kj}}{2\bar{v}_{Az}\sum_{k=1}^{n_r}\sum_{j=1}^{n_\theta}A_{z,kj}} \tag{3}$$

where $v_{z,jk}$ is the axial velocity of element (k,j) in the fan's rotor region, $A_{z,kj}$ is the area of element (k,j) normal to the axial direction and $\bar{v}_{Az}$ is the area-weighted average axial velocity given by Eq. (4).

$$\bar{v}_{Az} = \frac{\sum_{k=1}^{n_r}\sum_{j=1}^{n_\theta} v_{z,kj}A_{z,kj}}{\sum_{k=1}^{n_r}\sum_{j=1}^{n_\theta}A_{z,kj}} \tag{4}$$

The volumetric performance of each individual fan is quantified using a volumetric effectiveness metric (ξ_i), shown in Eq. (5).

$$\xi_i = \frac{\bar{v}_{Az,i}}{\bar{v}_{Az,id}} \tag{5}$$

where $\bar{v}_{z,i}$ is the area-weighted average axial velocity through fan (i) and $\bar{v}_{Az,id}$ is the "ideal" area-weighted average axial velocity through the fan with the most uniform axial velocity (highest uniformity index) within the dataset.

The flap-wise bending moment distribution ($\mathbf{M}_{z,\theta}$) was used to evaluate the fan blade loading [7,13]. The differential axial forces ($\delta f_{Z,kj}$, refer to Eq. (1)) exerted on each of the rotor region elements were used to calculate the flap-wise bending moment distribution ($\mathbf{M}_{z,\theta}$) in the fan's plane of rotation as shown in Eq. (6).

$$m_{z,j} = \sum_{k=1}^{n_r}\delta f_{z,kj}(r_{kj} - r_h) \text{ for } j = 1, \ldots, n_\theta \tag{6}$$

where $m_{z,j}$ is the j^{th} entry of the $\mathbf{M}_{z,\theta}$ array, $r_{k,j}$ is the radius to the centre of element (k,j) and r_h is the fan hub radius.

The peak bending moment (M_p) (Eq. (7)) of this flap-wise bending moment distribution ($\mathbf{M}_{z,\theta}$) was used as the indicator of the severity of dynamic blade loading. Venter [15] found this metric to provide the best correlation to experimental dynamic blade loading trends.

$$M_p = \max\left(\left|\mathbf{M}_{z,\theta}\right|\right) \tag{7}$$

This peak bending moment is normalised with the peak bending moment at the "ideal" most uniform inlet airflow condition ($M_{p,id}$, the peak bending moment at $\bar{v}_{Az,id}$) as shown in Eq. (8).

$$\phi_i = \frac{M_{p,i}}{M_{p,id}} \tag{8}$$

VALIDATION DATA

Measurement specifics

The details on the experimental validation data used in this study are discussed in the project report compiled by Maulbetsch and DiFilippo [2]. The experimental measurements were not conducted as part of this study but were obtained from the parties involved in the aforementioned study [2]. The on-site tests discussed in this report were conducted at a power plant that utilises a 3 × 6 cell ACC (as shown in Figure 5) with the same axial fan as was used in the numerical CFD-based model. Measurements that were recorded over a period of three days were used for this evaluation. The wind direction within this time period was predominantly south-westerly to north-westerly.

Of the recorded data, only the anemometer and blade loading measurements for the edge fan cell indicated in Figure 5 was used. The location of the anemometers within this fan cell's inlet shroud is shown in Figure 5. The blade loading was measured simultaneously using load cells installed at the retaining bolts of six of the nine fans. Data from only one of these load cells was used in this study. The raw data (from the anemometers and the load cell) was processed into average and standard deviation values, calculated over three-minute interval segments.

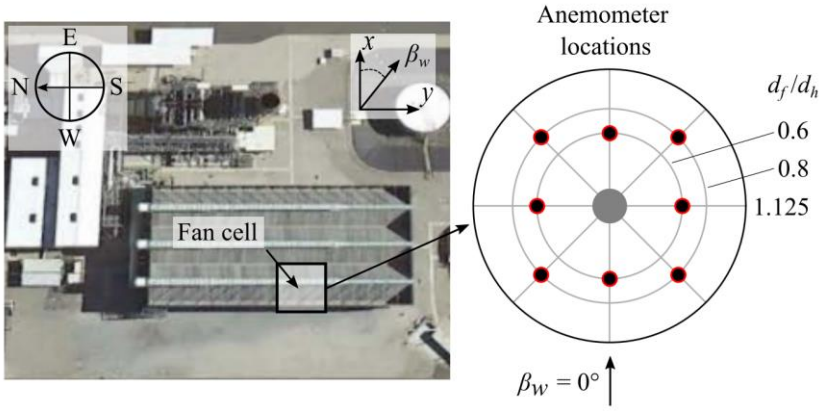

Figure 5:ACC facility layout and anemometer measurement locations (adapted from [2])

Experimental evaluation metrics

For the experimental measurements, the uniformity index was quantified using the average axial velocity ($\bar{v}_z$) of the eight anemometer measurements ($n_a = 8$) and not the area-weighted average ($\bar{v}_{Az}$). Therefore, the experimental uniformity index (γ_{ex}) is calculated using Eq. (9) (derived from Eq. (3)).

$$\gamma_{ex} = 1 - \frac{\sum_{j=1}^{n_a} |v_{z,j} - \bar{v}_z| / n_a}{2\bar{v}_z} \tag{9}$$

The volumetric performance of the experimental measurements is also presented in terms of volumetric effectiveness (ξ_{ex}, Eq. (5)) using the average axial velocity ($\bar{v}_z$) of the eight anemometer measurements. The dynamic blade loading for the experimental data is expressed as a normalised peak load (ϕ_{ex}) using Eq. (8). The standard deviation of the load cell measurement over the three-

minute interval (L_σ) can be converted to a peak load (L_p) using Eq. (10) based on the assumption that the signal is purely sinusoidal.

$$L_p = L_\sigma \sqrt{2} \tag{10}$$

RESULTS

Uniformity index

Figure 6 depicts the numerically predicted individual fan cell volumetric effectiveness (ξ_i, Eq. (5)) and uniformity index (γ_i, Eq. (3)) respectively, for the 3 × 6-cell ACC with a dimensionless platform height of H_p/d_f = 1.353 with a wind speed of v_w = 7 m/s.

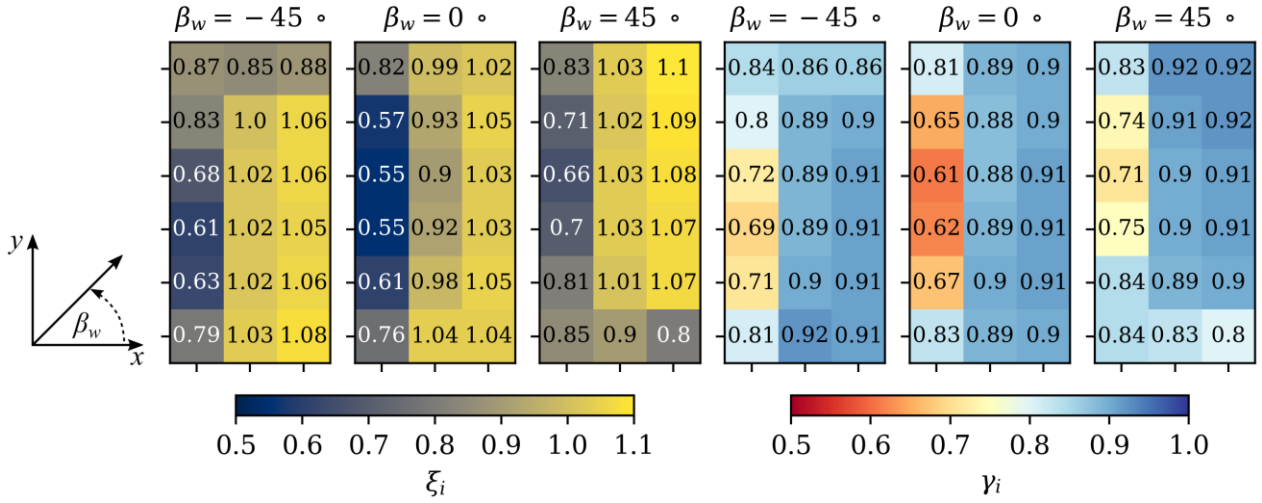

Figure 6: Numerically predicted individual fan cell volumetric effectiveness (ξ_i) and individual fan cell uniformity index with changing wind direction (v_w = 7 m/s; H_p/d_f = 1.353)

Figure 6 shows that uniformity index (γ_i) exhibits a very similar trend to fan volumetric effectiveness (ξ_i). This is expected as the uniformity index quantifies the variation between the mean axial velocity of the fan model's rotor region and the axial velocity of the individual blade elements of the rotor region. Thus, with a uniformity index close to unity, the axial velocity is expected to be uniform, and therefore the fan is likely operating close to design or "ideal" conditions ($\xi_i \rightarrow 1$). A decreasing uniformity index infers that the fan is subjected to distorted inlet conditions, which are known to negatively impact the volume flow rate through the fan ($\xi_i < 1$).

Figure 7 shows the numerically predicted individual fan uniformity index (γ_i) compared to (a) volumetric effectiveness (ξ_i) and (b) normalised peak bending moment (ϕ_i, Eq. (8)). The figure shows results for all 18 fans across the range of wind speeds ($1 \leq v_w \leq 11$ m/s) and directions ($-90^\circ \leq \beta_w \leq 90^\circ$) simulated. A total of 972 fan cell operating points are included in Figure 7. The figure also includes a mean trendline ($f_m(\gamma)$), used as the reference comparison against the validation data (this is purely for a comparative purpose, and thus the equations for the trendlines are omitted).

Figure 7 shows a definite relationship between fan uniformity index and volumetric effectiveness. Normalised peak bending moment increases rapidly with decreasing γ_i reaching a maximum at $\gamma_i \approx 0.85$, after which the influence of γ_i decays and eventually plateaus. The plateau is likely due to the fan inlet velocity vectors (specifically axial velocity) in the upwind half of the fan's rotational plane reaching conditions that lead to a loading scenario that cannot necessarily get much worse.

Figure 8 shows the uniformity index calculated using the experimental validation data (γ_{ex}, Eq. (9)) compared to (a) the experimental volumetric effectiveness (ξ_{ex}) and (b) experimental normalised

peak loading (ϕ_{ex}) for the upwind edge fan as indicated in Figure 5. The figure includes the numerical trend line ($f_m(\gamma)$). From Figure 8, it is clear that the uniformity index (γ_{ex}) and volumetric effectiveness (ξ_{ex}) calculated from the experimental validation data follows a similar trend seen in the numerical data ($f_m(\gamma)$, Figure 7).

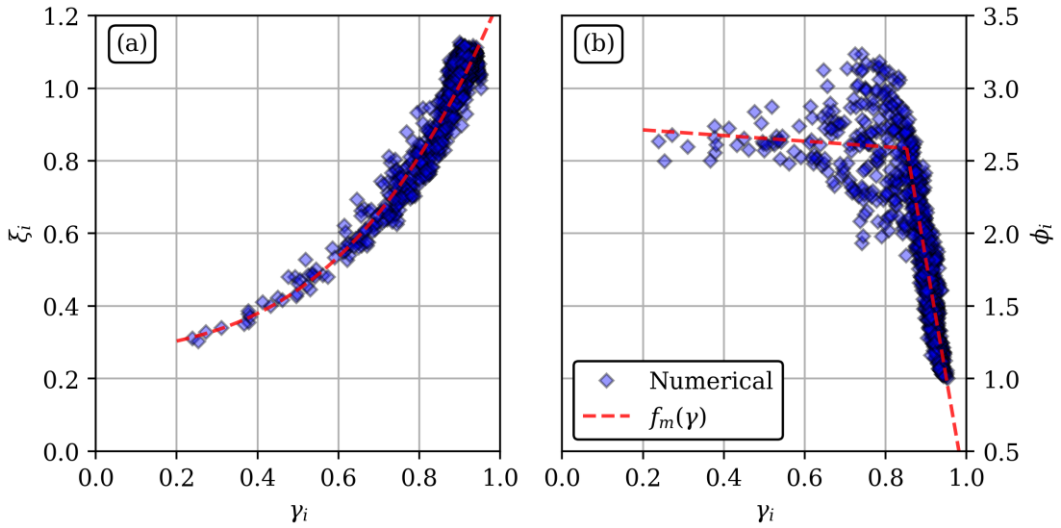

Figure 7: Individual fan cell uniformity index (γ_i) compared to (a) volumetric effectiveness (ξ_i) and (b) normalised peak bending moment (ϕ_i) (H_p/d_f = 1.353)

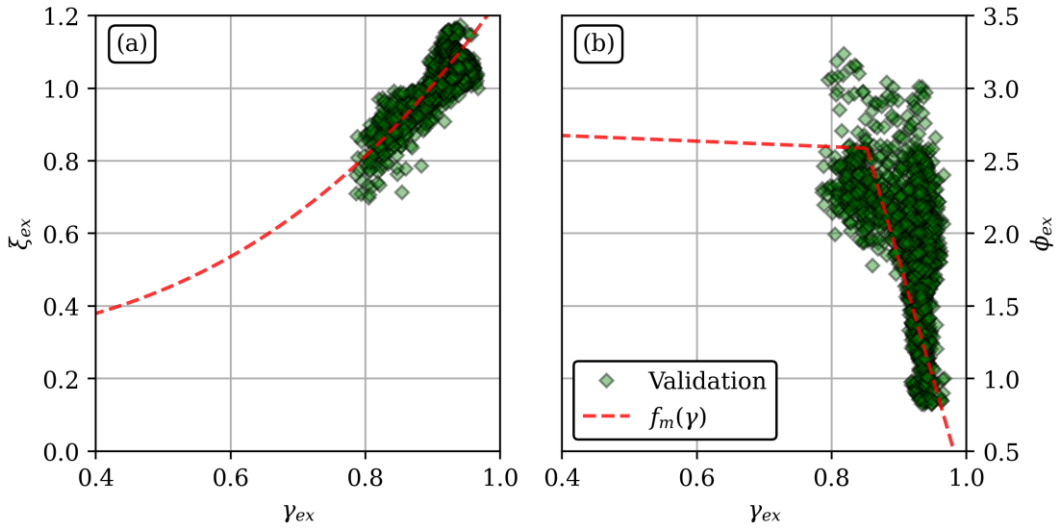

Figure 8: Experimentally measured uniformity index (γ_{ex}) compared to (a) volumetric effectiveness (ξ_{ex}) and (b) normalised peak bending moment (ϕ_{ex}) (H_p/d_f = 1.353)

Sensitivity of uniformity index to sampling resolution

Uniformity index is calculated using the measured axial velocities at grid points within a polar coordinate grid. Changing the sampling resolution will thus influence the calculation of the uniformity index. This effect was investigated by interpolating the per grid point axial velocity of the original grid (n_r = 20; n_θ = 120 grid resolution) onto a coarser resolution and recalculating the uniformity index (Eq. (3)) from the numerical results. The sample location for the coarser uniformity index calculation within the fan rotor is shown in Figure 9. Figure 9 (c) is the minimum measurement resolution of the CTI-PTG-143 standard.

The recalculated uniformity index results are shown in Figure 10 for four different grid resolutions, starting at the far left with the original (n_θ = 120; n_r = 20) for a wind speed of v_w = 7 m/s with a direction of β_w = 0˚. Figure 10 indicates that for this specific test case (v_w = 7 m/s; β_w = 0˚),

changing the sampling resolution has an effect. However, this is only significant at very low resolutions such as (d). Furthermore, with a low tangential resolution as with (c) and (d), it can be expected that an alternative wind direction not radially aligned with sampling locations (i.e. $\beta_w = 45^\circ$) would reduce the accuracy of the uniformity index calculation further. This effect is not noticeable in Figure 10 due to the wind direction being radially aligned with sampling locations.

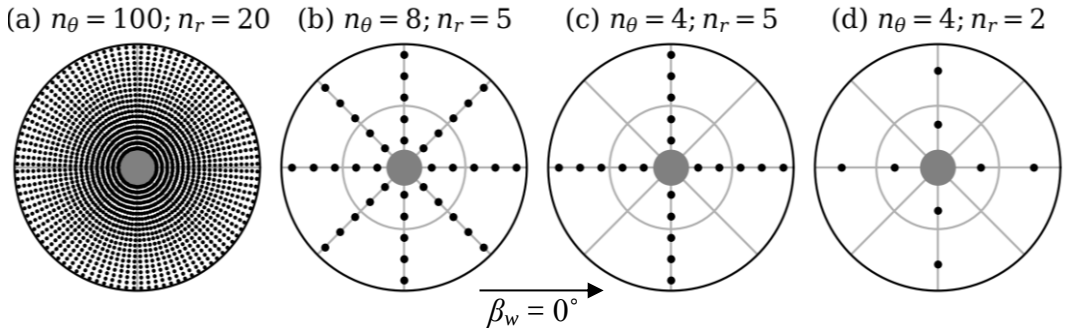

Figure 9: Sampling resolution used for calculating uniformity index

This discussion indicates that a detailed investigation into identifying the lowest optimal measurement resolution and configuration for on-site experimental measurement of uniformity index would be of value.

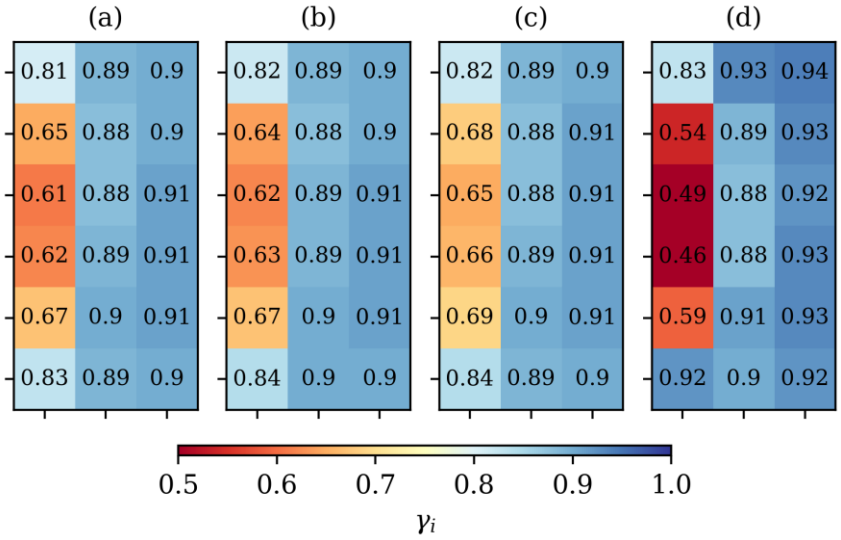

Figure 10: The influence of changing grid resolution on the calculation of uniformity index (v_w = 7 m/s; $\beta_w = 0^\circ$; H_p/d_f = 1.353)

CONCLUSIONS

The uniformity of an ACC fan's axial velocity inflow was identified as a metric of interest in terms of quantifying ACC fan operation under windy conditions. This paper evaluated fan inflow uniformity index using a numerical CFD-based approach which was validated against on-site experimental measurements.

The simulation results from the numerical ACC model indicated that there is a proportional relationship between uniformity index and both fan volumetric effectiveness and dynamic blade loading. Fan inlet airflow uniformity index (γ) can thus be used to estimate the severity of both the reduction in fan volumetric performance and the increase in dynamic blade loading under windy conditions. This same proportional relationship was observed in the experimental validation data,

suggesting that uniformity index can be used in both numerical and experimental work to allow for a qualitative investigation and specification of wind effects and wind effect mitigation mechanisms.

The potential utility of uniformity index in numerical simulation is that the state of fan blade dynamic loading can be inferred without additional data processing or a blade element theory-based fan model. For continuous on-site experimental measurements, a uniformity index can indicate a fan cell's volumetric performance and dynamic blade loading using significantly less measurement equipment (less than 40 anemometers and no need for strain gauges, bridge amplifier and a wireless transmitter). Furthermore, uniformity index can improve the utility of on-site experimental measurements as uniformity index can give a much clearer indication of the severity of wind effects or cross-flow effects at an ACC than an arbitrary windspeed measurement that can be influenced by surrounding buildings and the induced draft of the ACC fans.

ACKNOWLEDGEMENTS

The authors acknowledge the financial support provided to this project by Stellenbosch University's Solar Thermal Energy Research Group and the computational resources provided by the Centre for High-Performance Computing (CHPC), South Africa.

REFERENCES

[1] J.S. Maulbetsch, M. DiFilippo, *Effect of wind speed and direction on the performance of air-cooled condensers*, California Energy Commission, Publication Number: CEC-500-2013-065-APB, **2008**.

[2] J.S. Maulbetsch, M. DiFilippo, *The use of wind barriers to mitigate the effect of wind on air-cooled condensers*, California Energy Commission, Publication number: CEC-500-2016-047, **2016**.

[3] J.R. Bredell, D.G. Kröger, G.D. Thiart, *Numerical investigation of fan performance in a forced draft air-cooled steam condenser*, Appl. Therm. Eng. 26, pp. 846–852, **2006**. https://doi.org/10.1016/j.applthermaleng.2005.09.020.

[4] G.D. Thiart, T.W. von Backström, *Numerical simulation of the flow field near an axial flow fan operating under distorted inflow conditions*, J. Wind Eng. Ind. Aerodyn. 45, pp. 189–214, **1993**. https://doi.org/10.1016/0167-6105(93)90270-X.

[5] C.J. Meyer, *Numerical investigation of the effect of inlet flow distortions on forced draught air-cooled heat exchanger performance*, Appl. Therm. Eng. 25, pp. 1634–1649, **2005**. https://doi.org/10.1016/j.applthermaleng.2004.11.012.

[6] W.H. Stinnes, T.W. von Backström, *Effect of cross-flow on the performance of air-cooled heat exchanger fans*, Appl. Therm. Eng. 22, pp. 1403–1415, **2002**. https://doi.org/10.1016/S1359-4311(02)00060-1.

[7] P.J. Hotchkiss, C.J. Meyer, T.W. von Backström, *Numerical investigation into the effect of cross-flow on the performance of axial flow fans in forced draught air-cooled heat exchangers*, Appl. Therm. Eng. 26, pp. 200–208, **2006**. https://doi.org/10.1016/j.applthermaleng.2005.05.012.

[8] F.S. Marincowitz, *Experimental investigation of the effects of windscreens on air- cooled condenser fan performance and dynamic blade loading*, University of Stellenbosch, **2019**. https://doi.org/10.13140/RG.2.2.24964.65929/1.

[9] J. Muiyser, D.N.J. Els, S.J. van der Spuy, A. Zapke, *Measurement of air flow and blade loading at a large-scale cooling system fan*, J. South African Inst. Mech. Eng. 30, pp. 30–38, **2014**.

[10] Cooling Tower Institute, *CTI Standard PTG-143: Recommended Practice For Airflow Testing of Cooling Towers*, **1994**.

[11] L.J. Yang, X.Z. Du, Y.P. Yang, *Wind effect on the thermo-flow performances and its decay characteristics for air-cooled condensers in a power plant*, Int. J. Therm. Sci. 53, pp. 175–187, **2012**. https://doi.org/10.1016/j.ijthermalsci.2011.10.021.

[12] F.S. Marincowitz, M.T.F. Owen, J. Muiyser, *The Effect of Windscreens and Walkways On Air-cooled Condenser Performance and Fan Blade Dynamic Loading*, J. Eng. Gas Turbines Power. 143, **2021**. https://doi.org/10.1115/1.4051640.

[13] J.R. Bredell, D.G. Kröger, G.D. Thiart, *Numerical investigation into aerodynamic blade loading in large axial flow fans operating under distorted inflow conditions*, J. South African Inst. Mech. Eng. 22, pp. 11–17, **2006**.

[14] C. Bianchini, G. Mirsky, M. Frumkin, *Windscreen effect on performance and structure, before and after, and comparison with CFD*, in: ACC User Gr., Colorado Springs, CO, **2018**.

[15] A.J. Venter, *Numerical analysis of windscreen effects on air-cooled condenser fan performance and blade loading*, University of Stellenbosch, **2020**. https://doi.org/10.13140/RG.2.2.34819.73768.

[16] J. Franke, C. Hirsch, G. Jensen, H.W. Krüs, S.D. Miles, M. Schatzmann, P.S. Westbury, J.A. Wisse, N. Wright, *Recommendations on the use of CFD in wind engineering*, in: Proc. Int. Conf. Urban Wind Eng. Build. Aerodyn., Von Karman Institute for Fluid Dynamics, Sint-Genesius-Rode, pp. C.1.1-C1.11, **2004**.

[17] P.J. Richards, R.P. Hoxey, *Appropriate boundary conditions for computational wind engineering models using the k-ε turbulence model*, J. Wind Eng. Ind. Aerodyn. 46–47, pp. 145–153, **1993**. https://doi.org/10.1016/0167-6105(93)90124-7.

[18] R.A. Engelbrecht, C.J. Meyer, J. van der Spuy, *Modeling Strategy for the Analysis of Forced Draft Air-Cooled Condensers Using Rotational Fan Models*, J. Therm. Sci. Eng. Appl. 11, **2019**. https://doi.org/10.1115/1.4042590.

[19] A.J. Venter, M.T.F. Owen, J. Muiyser, *A numerical analysis of windscreen effects on air-cooled condenser fan performance*, Appl. Therm. Eng. 186, **2021**. https://doi.org/10.1016/j.applthermaleng.2020.116416.

[20] D.G. Kröger, *Air-cooled heat exchangers and cooling towers: Thermal-flow performance evaluation and design*, PennWell Corporation, Tulsa, **2004**.

[21] W.M. Kays, A.L. London, *Compact heat exchangers*, 3 rd, McGraw-Hill, New York, **1984**.

[22] F.S. Marincowitz, *Optimisation towards a wind-resistant air-cooled condenser for the modern energy sector*, University of Stellenbosch, **2021**. https://doi.org/10.13140/RG.2.2.13144.83200/1.

[23] S.J. van der Spuy, T.W. von Backström, *An evaluation of simplified CFD models applied to perimeter fans in air-cooled steam condensers*, Proc. Inst. Mech. Eng. Part A J. Power Energy. 229, pp. 948–967, **2015**. https://doi.org/10.1177/0957650915594073.

[24] ANSYS Inc., *ANSYS Fluent theory guide*, Release 15.0, **2013**.